Superfluid fraction of few bosons in an annular geometry in the presence of a rotating weak link

Alex V. Andriati [*] and Arnaldo Gammal [†]
Instituto de Física, Universidade de São Paulo, 05508-090 São Paulo, Brazil

(Received 1 August 2019; published 12 December 2019)

We report beyond mean-field many-body calculations of ground-state mass current and superfluid fraction for a system of few bosons confined in a ring geometry in the presence of a rotating weak link induced by a potential barrier. We apply the multiconfiguration Hartree method for bosons to do beyond mean-field calculations of the average superfluid fraction for various barrier heights, interaction strengths, and number of particles. This approach presents us a way to continuously sweep the interaction from a weak to strong case. For different rotating frequencies, the ground-state energy remains periodic but with a different landscape depending on the barrier height, and this periodicity implies a decrease on the mass current for fast rotating barriers. With the rotation frequency close to zero, our results show that by sufficiently increasing the barrier, the superfluid fraction eventually drops to zero regardless of interaction strength and number of particles. Also, the condensate fraction depends almost exclusively on the interaction strength, which shows independence of superfluidity and condensation. We also obtained correlation functions to explain the superfluidity behavior, which is not possible in the mean-field theory. This may be relevant to new devices based on atomtronics.

DOI: 10.1103/PhysRevA.100.063625

I. INTRODUCTION

The concepts of superfluidity [1–3] and Bose-Einstein condensation [4,5] have dominated the research of cold bosonic systems. The presence of one does not necessarily imply the other—whereas superfluidity is related to dissipationless flow due to a minimum required energy to create excitations, Bose-Einstein condensation is characterized by a single macroscopically occupied state. Superfluid systems with a very small condensation fraction around 10%, like liquid helium, are widely known [6,7], thereby characterizing independent effects.

Nevertheless, many reports explore the superfluidity features of a Bose-Einstein condensate (BEC), as dilute cold bosonic gases are able to present both phenomena simultaneously [8]. Especially, persistent flow, a hallmark of superfluidity, has been reported for a BEC trapped in a ring shape format early [9] and later in [10] in the presence of a tunable weak link. This boosted the interest to quantitatively study all the properties for the system due to a possible connection and quantum analogy with a superconducting quantum interference device (SQUID) [11] that was experimentally implemented [12] generating Josephson junctions [13].

Ring geometries are very interesting to study persistent currents and quantum coherence. In the last few years, there has been much interest in ring condensates, especially in the context of the atomtronics field [14,15]. Many works studied several properties on imposing rotation for a BEC confined in a ring-shape geometry, observing hysteresis ("swallow tail loops") [16–19], excitation mechanisms [20–22], spin superflow [23,24], and superfluid fraction [25]. Former theoretical studies rely mostly on the Gross-Pitaevskii (GP) equation that set a clear limitation on controlling the interactions to suppress the depletion from the condensate [26,27]. This has changed in the past few years with the development of methods able to compute many-body observables (generally correlation functions) and assure correctness for a wider range of interaction values [28–32].

The employment of new methods paves a way to study independently the condensation phenomena and the superfluidity for a system of cold bosonic atoms and to sweep a wider range of interaction strengths since depletion is included in the description. Moreover, they enable us to have a deep understanding of the physical system through new many-body quantities unseen in the mean-field formalism, like correlations, which has gained importance due to experimental measurements in the past decade for cold atomic clouds [33–36].

Specifically, the multiconfiguration time-dependent Hartree method for Bosons (MCTDHB) [31] has gained attention for its quite straightforward generalization of the GP equation, since it is still based on variational principles but with more time-dependent single-particle states (also known as orbitals) the atoms can occupy, therefore allowing the expansion of the many-body state in a configuration basis (Fock states) with each possible configuration expressed by a well-defined occupation number of the single-particle states. This procedure truncates the Hilbert space, whereas the coefficients of the basis expansion and the orbitals are determined by minimizing the action, enforcing an optimized basis. The MCTDHB has shown to be a powerful tool for many applications, for instance, to study quench dynamics in optical lattices [37–45] and other applications [46–48] as well as a version for fermions [49–53].

In the present paper, we study beyond mean field the superfluid fraction of a gas of few bosons at zero temperature in the presence of a tunable weak link moving in a periodic system

[*] andriati@if.usp.br
[†] gammal@if.usp.br

(an effective ring) using the MCTDHB to explore strong interactions and to show the loss of the superfluid fraction under a wide range of the physical parameters. For different rotating frequencies, we found that the ground-state energy remains periodic but with a different profile depending on the barrier height, and this periodicity implies a decrease on the current fraction for fast rotating barriers. With the rotation frequency close to zero, our results show that increasing sufficiently the barrier, the superfluid fraction eventually drops to zero regardless of the interaction strength and number of particles. Also, the condensate fraction depends almost exclusively on the interaction strength, which shows independence of superfluidity and condensation. Eventually, we obtain correlation functions to explain the superfluidity behavior, which is not possible in the mean-field theory.

The paper is structured as follows. In Sec. II, we present the model with the main equations; in Sec. III we show the periodicity in the energy spectrum and we define the superfluid fraction. In Sec. IV, we show the decrease of the superfluid fraction due to the increase of the barrier height and calculate the first-order correlations. Finally, in Sec. V we present the conclusions.

II. MODEL AND METHODS

The specific form of a barrier is generally unknown from an experimental perspective, though we must be able to define it through its thickness and height. As most experiments use lasers to physically implement a barrier [10], the height in the model plays the principal role as it is directly related to the laser beam intensity, while the thickness is determined by the laser beam width. An approach based on Dirac delta function for the barrier has been reported [54], which implies zero thickness. In any case, for a barrier rotating with velocity v, in the laboratory frame we thus have the one-body term of the Hamiltonian in the general form

$$\hat{h}(t) = -\frac{\hbar^2}{2m}\frac{\partial^2}{\partial \bar{x}^2} + U(\bar{x} - vt)\,, \quad \bar{x} \in (-\pi R, \pi R], \tag{1}$$

for a ring of radius R, where a specific form for U is chosen in Sec. III. The two-body part is assumed to be described by an effective contact interaction $V(\bar{x} - \bar{x}') = g_{1D}\delta(\bar{x} - \bar{x}')$, where g_{1D} is related to the transverse harmonic trap frequency and the scattering length of the atoms [55]. Using the unitary transformation to move to the rotating frame, $\exp(vt\partial/\partial x)$, the time dependence of Eqs. (1) is removed, resulting in the following many-body Hamiltonian in the second quantized formalism:

$$\mathcal{H} = \int_{-\pi R}^{\pi R} dx\, \hat{\Psi}^\dagger(x)\left[\frac{\hbar^2}{2m}\left(i\frac{\partial}{\partial x} + \frac{mv}{\hbar}\right)^2 + U(x)\right]\hat{\Psi}(x) + \frac{g_{1D}}{2}\int dx\, \hat{\Psi}^\dagger(x)\hat{\Psi}^\dagger(x)\hat{\Psi}(x)\hat{\Psi}(x), \tag{2}$$

where $x = \bar{x} - vt$ and $\hat{\Psi}(x)$ is the bosonic field operator.

The MCTDHB is developed assuming a truncated Hilbert space where the many-body state is a superposition of all possible configurations N_c of N particles distributed over M single-particle states, such that we can write

$$|\Psi(t)\rangle \doteq \sum_{\alpha=1}^{N_c} C_\alpha(t)|\vec{n}^{(\alpha)}\rangle, \quad N_c = \binom{N+M-1}{M-1}, \tag{3}$$

where each configuration $|\vec{n}^{(\alpha)}\rangle$ is a Fock state which satisfies $\sum_i^M n_i^{(\alpha)} = N$ for any α, and $n_i^{(\alpha)}$ is the occupation number of the single-particle state $\phi_i(x,t)$. Additionally, the single-particle states must satisfy the orthogonality condition $\int dx \phi_l^*(x,t)\phi_k(x,t) = \delta_{lk}, \forall k, l = 1, ..., M$. Using this ansatz, the time-dependent equations can be extracted from the minimization of the action with respect to the coefficients C_α in Eqs. (3) and the single-particle states, with the action defined by

$$\mathcal{S}[\mathbf{C}, \{\phi_k, \phi_k^*\}] = \int dt \left[\langle\Psi(t)|\dot{\Psi}(t)\rangle - \langle\Psi(t)|\mathcal{H}|\Psi(t)\rangle - \sum_{k,l=1}^{M}\mu_{kl}(t)\langle\phi_k|\phi_l\rangle_t\right], \tag{4}$$

where the μ_{kl} are introduced as Lagrangian multipliers to maintain orthonormality of the single-particle states. The variational principle conducts to M nonlinear coupled partial differential equations for the set $\{\phi_k(x,t)\}$ and a system of N_c ordinary differential equations for the coefficients C_α [31,56]. It is worth mentioning that the GP equation is a special case where we have just one possible configuration $|\vec{n}\rangle = |N, 0, ..., 0\rangle$, that yields for the macroscopically occupied orbital $\phi(x,t)$ the equation

$$i\hbar\frac{\partial\phi(x,t)}{\partial t} = [\hat{h}' + g_{1D}(N-1)|\phi(x,t)|^2]\phi(x,t), \tag{5}$$

with $\hat{h}' = \hbar^2/2m(i\partial/\partial x + mv/\hbar)^2 + U(x)$ the one-body Hamiltonian in the rotating frame.

For numerical simulation purposes, we assume the following system of units: length measured in units of (πR), density probability/particle in units of $(\pi R)^{-1}$ and energy by $\hbar\zeta$, where $\zeta = (\hbar/2m\pi^2R^2)$. Moreover, we introduce the dimensionless parameters $\Omega = mRv/\hbar$ and $\gamma = 2m\pi R g_{1D}/\hbar^2$. In numerical computations, all these transformations yield the orthonormalization condition for the set of orbitals $\int_{-1}^{1} dx\phi_l^*(x,t)\phi_k(x,t) = \delta_{lk}$, where x must be interpreted in units of πR in the simulations. Here we developed our own codes to solve the MCTDHB equations with periodic boundary conditions. Our codes were extensively tested, matching the results of the examples of the code available in Ref. [57], which has produced many results [39,46–49]. We adjusted the number of single-particle states until the energy converged in at least four decimal places.

III. PERIODICITY IN ENERGY SPECTRUM AND DEFINITION OF SUPERFLUID FRACTION

In the absence of a barrier, the single-particle energy levels as a function of Ω are parabolas given by $E_j/(\hbar\zeta) = (j - \Omega)^2\pi^2$, each one defined by the winding number of the phase (j), centered at $\Omega_j = j$, and crossing each other at $\tilde{\Omega}_j = (j + 1/2)$ [18].

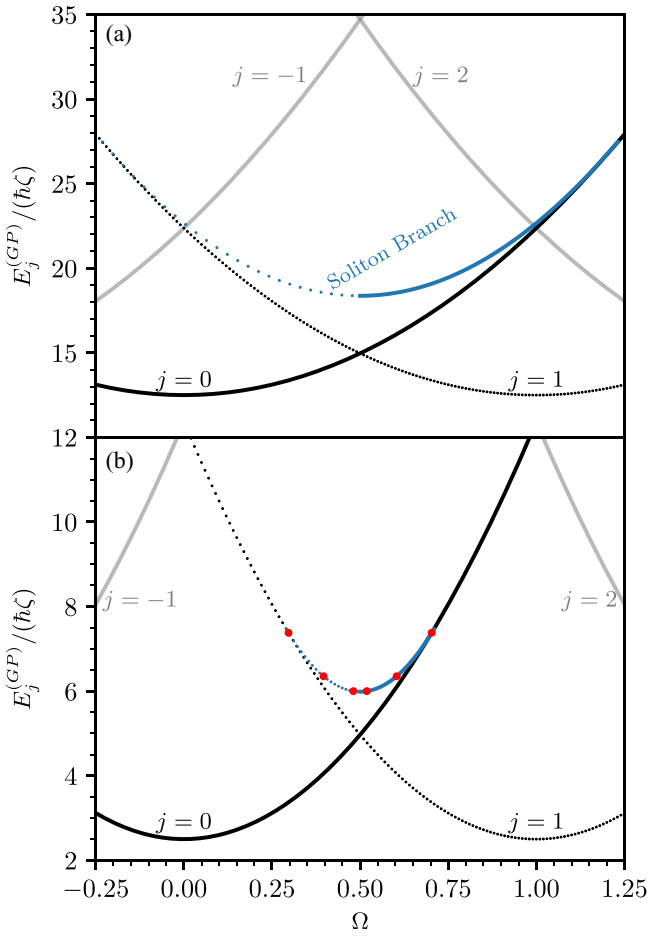

FIG. 1. Energy per particle from the GP equation as a function of Ω for different winding numbers (j) with (a) $\gamma(N-1)=50$ and (b) $\gamma(N-1)=10$. In both cases, the soliton's energy is depicted in blue, where the dotted part has winding number $j=1$ and the full line $j=0$, connecting with the parabolas with corresponding winding numbers. Other values of winding numbers are shown in gray. The rotation velocity values in the horizontal axis are in dimensionless units.

As a first approach, we use the GP equation once the interaction is included in the description. In this case, still in the absence of the barrier, there are two kinds of analytical solutions. One with constant density, which results in the same energy of thesingle-particle case, with the addition of an interaction contribution, yielding $E_j^{(\mathrm{GP})}/(\hbar\zeta)=(j-\Omega)^2\pi^2+\gamma(N-1)/4$ as average energy per particle. The other is a soliton given in terms of Jacobi elliptic functions [58,59] that exists for a finite range of values of Ω, where the extension of this range depends on the interaction strength. Figure 1 shows an energy landscape of the analytical solutions of the GP equation with the soliton solution energy connecting two parabolas from constant density solutions, where the dotted lines have winding number $j=1$ and the filled line $j=0$.

In Fig. 2, we present the phase of the soliton solutions. The soliton solutions exhibit a transition between different winding numbers and, for increasing Ω, a discontinuity in phase occurs at $\Omega=0.5$, going from $j=1$ to $j=0$. Moreover, these solutions yield what is known as a swallow-tail loop

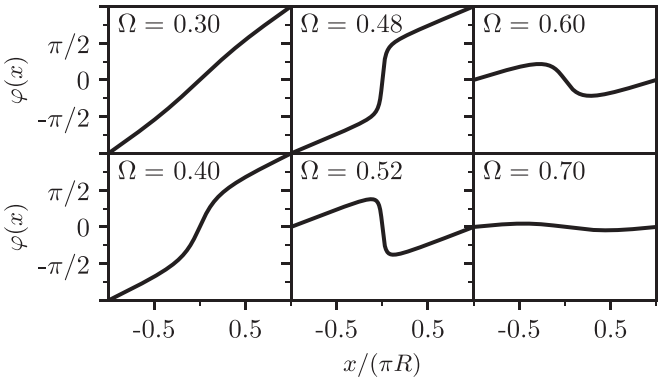

FIG. 2. Phase profile of the soliton solution $\varphi(x)$ for some values of Ω corresponding to the red dots in Fig. 1(b). An abrupt transition occurs at $\Omega=0.5$ that implies a transition in the winding numbers, from $j=1$ to $j=0$.

in the energy shown in Figs. 1(a) and 1(b), which is related to a hysteretic behavior [16–18,60]. The soliton branch in Fig. 1 is an excited state and will not be further discussed here, since the aim of the present paper is to measure the superfluid fraction of the ground state. In addition, Fig. 1 reveals that the ground-state energy has a periodic behavior with respect to the rotation Ω, with kinks where the parabolas cross each other at $\tilde{\Omega}_j=(j+1/2)$. This periodic structure remains even in the presence of a barrier, as will be shown later. An important fact is that we can relate the mass current circulation with the energy and use this periodicity to understand what happens to the current under the action of fast rotating barriers.

Here we start a derivation of mass current by looking at the time variation of the number of atoms within the range $[x_1,x_2]\subseteq[-\pi R,\pi R]$, as

$$\frac{d}{dt}\int_{x_1}^{x_2}dx\,\langle\Phi(t)|\hat{\Psi}^\dagger(x)\hat{\Psi}(x)|\Phi(t)\rangle = \frac{i}{\hbar}\int_{x_1}^{x_2}dx\,\langle[\mathcal{H},\hat{\Psi}^\dagger(x)\hat{\Psi}(x)]\rangle_t, \tag{6}$$

where $\langle\cdot\rangle_t$ means the expectation value for an arbitrary many-body state $|\Phi(t)\rangle$. Using Eq. (2) with the usual commutation relation for the boson field operator $[\hat{\Psi}(x),\hat{\Psi}^\dagger(x')]=\delta(x-x')$ to evaluate the commutator of the Hamiltonian with the density operator, the only terms that contribute are those carrying a derivative, and yield

$$[\hat{\Psi}^\dagger(x)\hat{\Psi}(x),\mathcal{H}] = -\frac{\hbar^2}{2m}\left(\hat{\Psi}^\dagger(x)\frac{\partial^2\hat{\Psi}(x)}{\partial x^2}-\frac{\partial^2\hat{\Psi}^\dagger(x)}{\partial x^2}\hat{\Psi}(x)\right) + i\hbar v\left(\hat{\Psi}^\dagger(x)\frac{\partial\hat{\Psi}(x)}{\partial x}+\frac{\partial\hat{\Psi}^\dagger(x)}{\partial x}\hat{\Psi}(x)\right). \tag{7}$$

It is straightforward to factor out the derivative with respect to x, and further using Eq. (7) in Eq. (6) yields

$$\frac{d}{dt}N([x_1,x_2];t)=-[\langle\hat{J}(x_2)\rangle_t-\langle\hat{J}(x_1)\rangle_t]\,, \tag{8}$$

where $N([x_1,x_2];t)\doteq\int_{x_1}^{x_2}dx\langle\Phi(t)|\hat{\Psi}^\dagger(x)\hat{\Psi}(x)|\Phi(t)\rangle$ is introduced and the particle number current operator $\hat{J}(x)$ is

given by

$$\hat{J}(x) = -\frac{i\hbar}{2m}\left(\hat{\Psi}^\dagger(x)\frac{\partial\hat{\Psi}(x)}{\partial x} - \frac{\partial\hat{\Psi}^\dagger(x)}{\partial x}\hat{\Psi}(x)\right) - v\hat{\Psi}^\dagger(x)\hat{\Psi}(x). \tag{9}$$

The reduced single-particle density matrix (1-RDM) defined by $n^{(1)}(x,x';t) \doteq \langle\hat{\Psi}^\dagger(x')\hat{\Psi}(x)\rangle_t$ [34] has as a set of eigenvalues and eingenstates defined by the solution of $\int_{-\pi R}^{\pi R} dx\ n^{(1)}(x,x';t)\psi(x',t) = \mathcal{N}(t)\psi(x,t)$, with $\mathcal{N}(t)$ the average occupation number in the eigenstate $\psi(x,t)$, here also called a *natural orbital*. Using these natural orbitals to express the reduced single-particle density matrix $n^{(1)}(x,x';t)$ allows us to express the current as a superposition, $\langle\hat{J}(x)\rangle_t = \sum_k j_k(x,t)$, where

$$j_k = -\left[\frac{i\hbar}{2m}\left(\psi_k^*\frac{\partial\psi_k}{\partial x} - \psi_k\frac{\partial\psi_k^*}{\partial x}\right) + v|\psi_k|^2\right]\mathcal{N}_k, \tag{10}$$

with the position and time arguments omitted.

For the ground state, the current $\langle\hat{J}(x)\rangle_t$ must be independent of position and time, because the density is not time dependent. If we further average it over a period in the counter direction of the barrier velocity, it yields

$$\langle\rho_s\rangle(v) = \tau\frac{1}{2\pi R}\int_{\pi R}^{-\pi R} dx\left(\frac{\langle\hat{J}\rangle}{N}\right), \tag{11}$$

where $\tau = 2\pi R/v$ is the period of barrier rotation. This quantifies the mean fraction of particles that go through the counterdirection of the barrier in one period, that is from πR to $-\pi R$ indicated by the limits of integration taken. Therefore, if $\langle\rho_s\rangle(v)$ takes the value 1, it means a perfect superfluid since all the particles are flowing with velocity $-v$ in the rotating frame, that is, they remain at rest for an observer in the laboratory frame. Relations with other observables can be established, for instance, using the average momentum per particle,

$$\langle\rho_s\rangle(v) = \left(1 - \frac{\langle\hat{p}\rangle}{mv}\right), \quad \hat{p} = -\frac{i\hbar}{N}\int_{-\pi R}^{\pi R} dx\ \Psi^\dagger(x)\frac{\partial}{\partial x}\Psi(x), \tag{12}$$

and a relation with the energy, by taking the derivative with respect to the barrier velocity:

$$\langle\rho_s\rangle(v) = \frac{1}{Nmv}\frac{\partial E}{\partial v}, \quad E = \langle\mathcal{H}\rangle. \tag{13}$$

The equation above can also be identified by the ratio between the moment of inertia of the atoms and the moment of inertia of a rigid body. Using $v = \omega R$ yields

$$\langle\rho_s\rangle(\omega) = \frac{1}{NmR^2}\left(\frac{1}{\omega}\frac{\partial E}{\partial\omega}\right) = \frac{I(\omega)}{I_{\rm cl}}. \tag{14}$$

The superfluid fraction at rest (or simply superfluid fraction), denoted here by $\langle\rho_s\rangle_0$ can be defined by taking the limit of $v \to 0$ in any of the forms Eqs. (11)–(13) or (14) and was studied in this way in previous works [2,3,25,61]. With the dimensionless system of units and parameters introduced at the end of Sec. II, we have a suitable expression for numerical calculations, defining $\epsilon \doteq E/(\hbar\zeta)$,

$$\langle\rho_s\rangle(\Omega) = \left(\frac{1}{2\pi^2 N\Omega}\frac{\partial\epsilon}{\partial\Omega}\right), \quad \langle\rho_s\rangle_0 \doteq \lim_{\Omega\to 0}\langle\rho_s\rangle(\Omega). \tag{15}$$

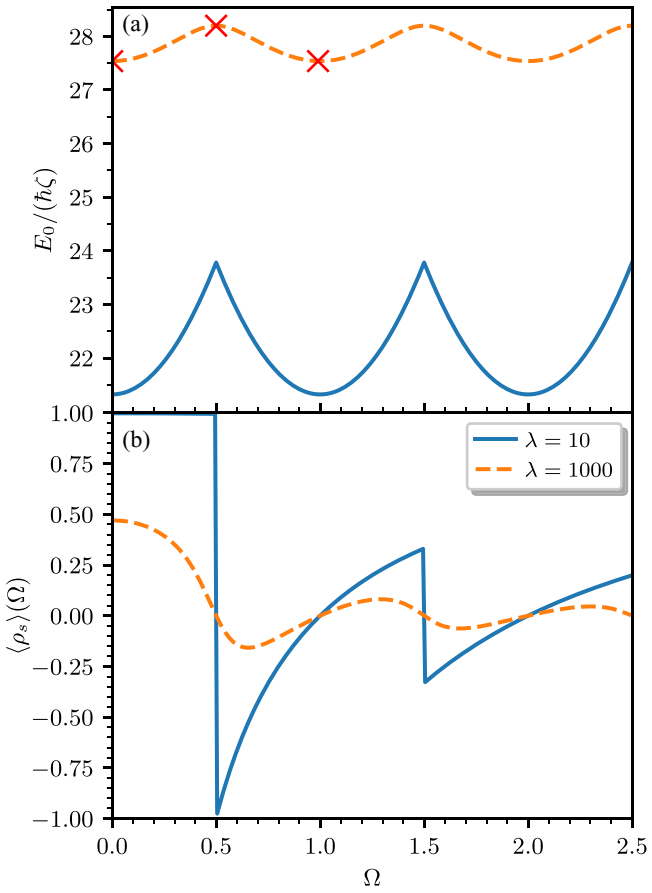

FIG. 3. Ground-state energy (a) and current fraction (b) for 11 particles as a function of dimensionless rotation velocity Ω in the rotating frame. The ground-state energy remains periodic as it was in Fig. 1 but with a different landscape depending on the barrier height λ, and this periodicity implies a decrease on the current fraction for fast rotating barriers. We used $\gamma = 10$ and $M = 5$ orbitals in the MCTDHB method.

Here we use the MCTDHB to find the ground state through imaginary time propagation for several parameters, and we first study the effect of rotation. Figure 3 illustrates the behavior of the energy in panel (a) and the current fraction in panel (b) as a function of the dimensionless barrier frequency Ω for two different barrier heights, where the specific form used in Eqs. (1) is

$$U(x) = \begin{cases} (\hbar\zeta\lambda)\cos^2\left(\frac{x}{2R\sigma}\right) & \text{if} \quad |x| \leqslant \pi R\sigma \\ 0 & \text{if} \quad \pi R \geqslant |x| > \pi R\sigma, \end{cases} \tag{16}$$

where λ denotes the barrier height in dimensionless units and the width of the barrier was taken fixed $\sigma = 0.1$.

The energy of the ground state in Fig. 3(a) has a period 1 with respect to dimensionless rotation frequency for both cases of weak and strong barriers, while the difference relies on the maximum that occurs at $\Omega_j = j$, that is, peaked or smooth. The superfluid fraction in Fig. 3(b) was computed using Eqs. (15) with finite differences to take the derivative. It shows a periodic behavior with a damped amplitude as function of Ω, due to the periodicity of energy. According to Eq. (15), the amplitude is damped by a factor of $1/\Omega$.

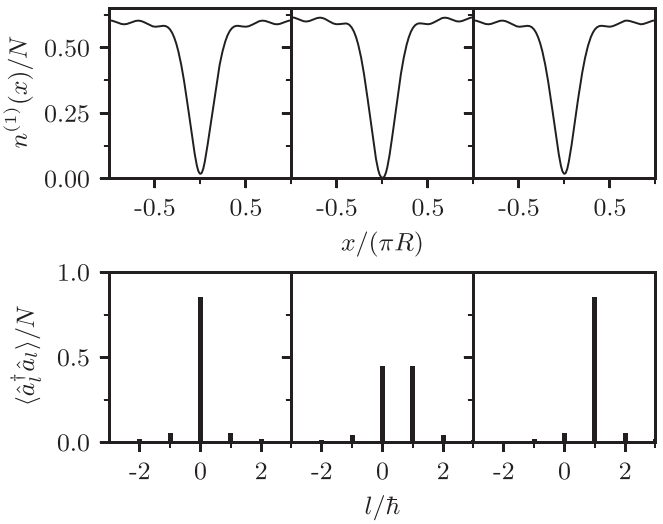

FIG. 4. Probability distribution as a function of position (upper panel) where $n^{(1)}(x) \doteq n^{(1)}(x,x) = \langle \hat{\Psi}^\dagger(x)\hat{\Psi}(x)\rangle$ and angular momentum distribution (lower panel) for barrier height $\lambda = 1000$. From left to right, $\Omega = 0, 0.5, 1.0$, corresponding to red crosses in Fig. 3. As used in Fig. 3, here $\gamma = 10$, $N = 11$ particles and $M = 5$ orbitals.

In the regions where $\langle \rho_s \rangle(\Omega) < 1$, the average momentum must increase together with the barrier velocity according to Eqs. (12). Indeed, that is what occurs in the lower panel of Fig. 4 that shows the angular momentum distribution for some values of Ω. Moreover, there is a critical dependence of the superfluid fraction on the barrier height, where Fig. 3 shows that, as Ω goes to zero, $\langle \rho_s \rangle(\Omega)$ diminishes when the barrier height is increased. This fact will be explored in the following.

IV. DECREASE OF SUPERFLUID FRACTION DUE TO INCREASE OF THE BARRIER HEIGHT

Numerical calculations of the superfluid fraction were carried out here using Eq. (13), finding the ground state by imaginary time propagation for $\Omega = 0$ and $\Omega = 0.02$, to approximate the derivative in $\Omega = 0.01$ and so get $\langle \rho_s \rangle(0.01)$. As shown by Fig. 3 the slope of current fraction goes to zero as $\Omega \to 0$, and therefore we use the value at $\Omega = 0.01$ as the proper superfluid fraction, assuming the difference of $\langle \rho_s \rangle_0 - \langle \rho_s \rangle(0.01)$ to be close to zero. To assure this method is valid, we compare with the result using Eqs. (12) at $\Omega = 0.02$ to check if there is no appreciable (less than 1%) variation on the estimation of superfluid fraction using a constant extrapolation of $\langle \rho_s \rangle(0.01)$.

In Fig. 5, we show the decrease of superfluid fraction for an increase in the barrier height in the form of Eq. (16), using a different number of particles and interaction strengths. Here the tunneling of particles through the barrier becomes harder as the barrier height is increased, thereby the system acquires momentum easily for higher barriers since it drags almost every particle with it. This easy momentum gain for very high barriers is responsible for the loss of superfluid fraction $\langle \rho_s \rangle_0$. It can also be noted that the superfluid fraction decreases more rapidly for fewer particles and lower interaction strengths; however, the number of particles and strength of interactions have a small impact in the form of the curves of $\langle \rho_s \rangle_0$ as a function of λ.

As can be seen in the upper panel of Fig. 6, the barrier height λ influences mostly the density at its peak, while the effect over the momentum distribution is a slight increase in its variance, but preserving the average angular momentum $\langle \hat{L} \rangle = 0$, as can be checked in the lower panel. Therefore, the angular momentum distribution is not very revealing about the behavior of the superfluid fraction at rest, different from the case for nonzero rotation shown in the lower panel of Fig. 4. Nonetheless, the density drastically changes as the barrier height increases, hence a more detailed study of 1-RDM, $\langle \hat{\Psi}^\dagger(x')\hat{\Psi}(x)\rangle$, will be done in the following.

It is worth noting that this loss of the superfluid fraction due to the increase in the barrier height is not related to the condensate fraction. As can be inferred from Table I, the condensate fraction depends mostly on the interaction strength and is minimally affected by the barrier height, particularly for small values of γ.

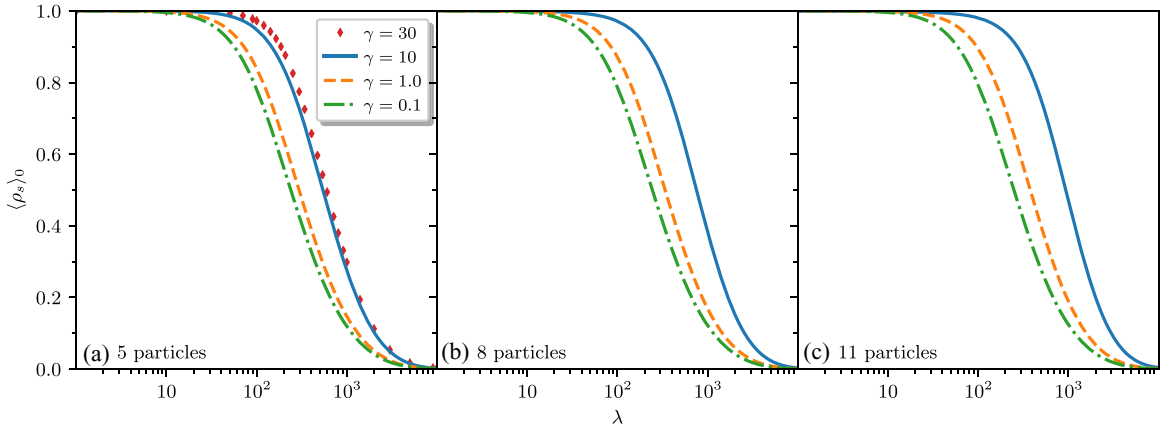

FIG. 5. Decrease of superfluid fraction for a different number of particles and interaction strengths (γ) due to increasing the barrier height (λ). All the cases share the common feature to be a perfect superfluid as the barrier becomes vanishing small, soon or later depending on the number of particles and interaction strength. For very high barriers, all particles are dragged together, imposing a rigid body rotation to the system. The number of orbitals was chosen as needed to converge the results, where for $\gamma \leqslant 10$, $M = 5$ was used while for $\gamma = 30$, $M = 9$ was needed. The barrier height values in the horizontal axis are in dimensionless units.

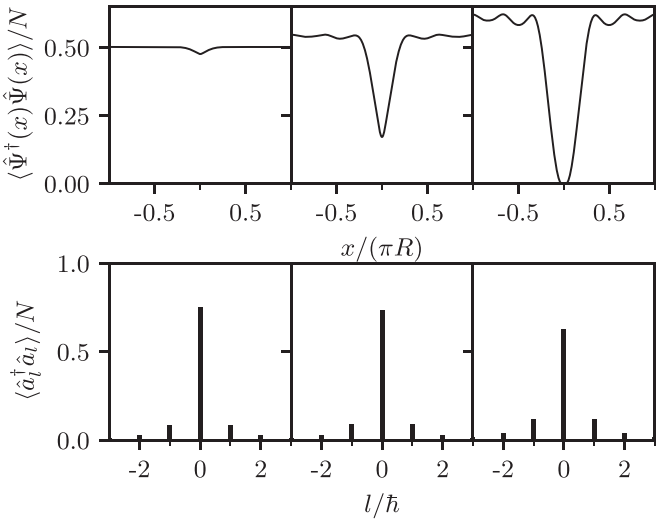

FIG. 6. Probability distribution of position (upper panel) and angular momentum (lower panel) for five particles, $\gamma = 30$ and different barrier heights $\lambda = 10, 200, 10\,000$ in the left, center, and right columns, respectively, in the absence of rotation $\Omega = 0$. The density distribution vanishes for $\lambda > 10^3$ at the peak of the barrier in $x = 0$, despite that there is just a slight increase on the width of the angular momentum distribution. As mentioned in Fig. 5, for $\gamma = 30$ we needed nine orbitals.

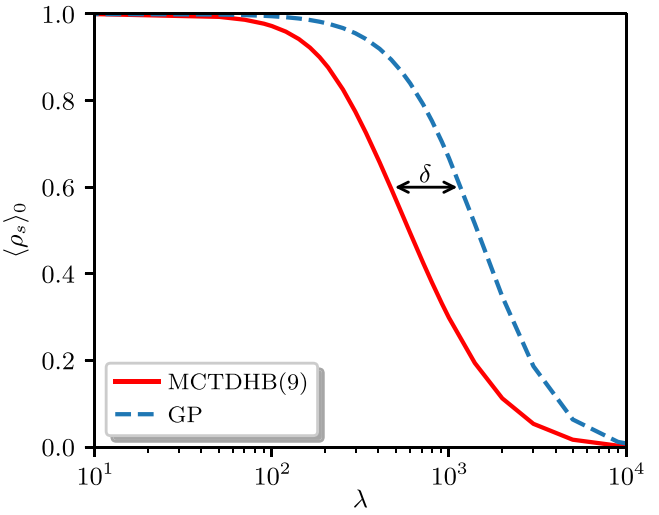

FIG. 7. Comparison between the superfluid fraction predicted by mean-field GP equation (dashed line) and the MCTDHB with nine orbitals (full line) for five particles and $\gamma = 30$, as function of barrier height λ. δ is the gap between the curves. The barrier height values in the horizontal axis are in dimensionless units.

We studied the difference between the MCTDHB and the mean-field theory as illustrated in Fig 7. In this case, the same values are predicted in the limits $\lambda \to 0$ and $\lambda \to \infty$; nonetheless, between these values of the barrier height, a large gap δ is found between the superfluidity curves. For instance, the height $\bar{\lambda}$ where $\langle\rho_s\rangle_0$ goes below 0.6 is $\bar{\lambda}_{\mathrm{MCTDHB}} \approx 468$ and $\bar{\lambda}_{\mathrm{GP}} \approx 1160$, resulting in an appreciable difference of $\delta \approx 692$. In another way to explore this difference, $\bar{\lambda}_{\mathrm{MCTDHB}} < \bar{\lambda}_{\mathrm{GP}}/2$ to have less than 60% of superfluid.

Being able to investigate many-body quantities beyond mean field, we further investigate how the tunneling amplitude is affected by the barrier height, that is, the transition amplitude for the system to move a particle from x to x'. This can be achieved by $|\langle\hat{\Psi}^\dagger(x')\hat{\Psi}(x)\rangle|^2$ weighted by the probabilities to find the particles in respective positions given by $n^{(1)}(x)$ and $n^{(1)}(x')$. This is directly related to the first-order normalized correlation function defined by [34,62]

$$g^{(1)}(x,x') = \frac{\langle\hat{\Psi}^\dagger(x')\hat{\Psi}(x)\rangle}{\sqrt{n^{(1)}(x)n^{(1)}(x')}}. \tag{17}$$

The values of $g^{(1)}$ shall be drastically affected by the barrier and must have an abrupt variation as $xx' > 0$ changes to $xx' < 0$, since the tunneling must be much harder if the shorter distance between two points has the barrier between them. Since the system is periodic, this discussion applies just at the vicinity of either x or x' being zero, because if $(x/\pi R)(x'/\pi R) = -1$, they are actually the same point in the ring.

The effect of barrier height mentioned above is in agreement with the images in Fig. 8 that maps $|g^{(1)}(x,x')|^2$ values to colors. In Fig. 8(a), in the presence of a weak barrier, it depends only on $|x - x'|$, while in Fig. 8(b) this symmetry is lost, with an abrupt variation near at the barrier peak, x or x' approximately zero. Therefore, high barriers split the image in four square blocks, with the darker regions (small normalized tunneling probabilities) located on $xx' < 0$. This is consistent with previous studies in Ref. [63], despite the different boundary conditions and interaction regimes.

We further stress the relevance of applying a method that allows us to compute many-body quantities since, for example, $|g^{(1)}(x,x')|^2$ would be identical 1 for all x and x' in case one uses the GP equation that corresponds to just one eigenstate of $n^{(1)}(x,x')$. Therefore, this first-order correlation function, besides its relation to the tunneling amplitude, provides us a measure of how well the system can be described by a product state that corresponds to the mean-field approach. In the ring studied, the higher the barrier the poorer the description by a product state.

TABLE I. Maximum/minimum condensate fraction given by the highest eingenvalue of $n^{(1)}(x,x')$, over the set of values of λ in Fig. 5. The maximum and minimum values for each case have little influence from the barrier height whereas the superfluid fraction maximum and minimum values go from 1 to 0, respectively. For $\gamma = 30$, we were able to perform the calculations only for five particles due to our code limitations. The number of orbitals used follows the ones mentioned in Fig. 5 depending on γ.

N/γ	1	10	30
11	0.9936/0.9920	0.92/0.89	
8	0.9946/0.9935	0.92/0.88	
5	0.9962/0.9956	0.91/0.88	0.75/0.70

V. CONCLUSIONS

We have thoroughly studied the superfluidity aspects of a gas of few bosons in ring geometry in presence of a rotating

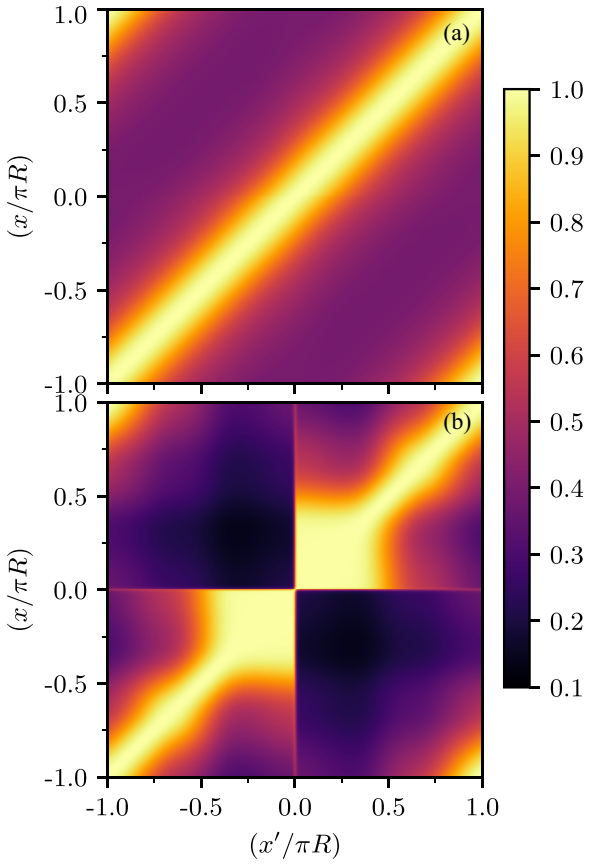

FIG. 8. $|g^{(1)}(x, x')|^2$ mapped to colors in the ring for five particles and $\gamma = 30$. Values of barrier heights used are $\lambda = 10$ in (a) and $\lambda = 10^4$ in (b) but sharing the same color scale. Here, nine orbitals were used in the numerical simulations.

barrier of variable height. We studied this system for different rotation frequencies, barrier heights, interaction strengths, and number of particles. For different rotating frequencies, the ground state energy remains periodic but with a different landscape depending on the barrier height, and this periodicity implies a decrease on the current fraction for fast rotating barriers. Another study with the rotation frequency close to zero allowed us to study the superfluidity of the stationary condensate. In this case, our results showed that by sufficiently increasing the barrier, the superfluid fraction eventually drops to zero regardless of interaction strength and number of particles. Also, we showed that condensate fraction depends almost exclusively on the interaction strength, which shows that both superfluidity and condensation are independent phenomena for the system.

The employment of MCTDHB allowed a continuous sweep in the interaction strength, without breaking in weak and strong interaction analysis [54,63], moreover, introducing many-body observables as correlation functions, which played an essential role to describe the loss of the superfluid fraction through the concept of tunneling. The effect of barrier height was studied regarding the correlation function $g^{(1)}(x, x')$. In the presence of a weak barrier, it depends only on $|x - x'|$, which means the tunneling is harder the longer the distance between the two points, while for a strong barrier this symmetry is lost, with an abrupt variation near the barrier peak.

All these features stress the relevance of the results, essentially for further practical purposes as quantum analogs of SQUIDS [10,12,17], with an accurate control of all parameters of the system. We emphasize that the results shown here can be related to further experiments, since the first-order correlation function was already explicitly measured [33] and a continuous amplification of interaction strength can be done using Feshbach resonance to prove the superfluid fraction curves.

ACKNOWLEDGMENTS

The authors thank the Brazilian agencies Fundação de Amparo à Pesquisa do Estado de São Paulo (FAPESP) (Grants No. 2018/02737 and No. 2016/17612-7) and Conselho Nacional de Desenvolvimento Científico e Tecnológico (CNPq) (Grant No. 306920/2018-2). We gratefully thank A. F. R. T. Piza, E. J. V. Passos, and R. K. Kumar for the elucidating discussions. We are also grateful for conversations with A. U. J. Lode and M. C. Tsatsos about the implementation of codes to numerically solve the MCTDHB equations.

[1] I. M. Khalatnikov, *An Introduction to the Theory of Superfluidity* (Advanced Book Program, Perseus Publisher, New York, 1965).
[2] A. J. Leggett, J. Stat. Phys. **93**, 927 (1998).
[3] A. J. Leggett, Rev. Mod. Phys. **71**, S318 (1999).
[4] M. H. Anderson, J. R. Ensher, M. R. Matthews, C. E. Wieman, and E. A. Cornell, Science **269**, 198 (1995).
[5] C. J. Pethick and H. Smith, *Bose-Einstein Condensation in Dilute Gases,* 2nd ed. (Cambridge University Press, Cambridge, 2008).
[6] O. Penrose and L. Onsager, Phys. Rev. **104**, 576 (1956).
[7] V. F. Sears, E. C. Svensson, P. Martel, and A. D. B. Woods, Phys. Rev. Lett. **49**, 279 (1982).
[8] C. Raman, M. Köhl, R. Onofrio, D. S. Durfee, C. E. Kuklewicz, Z. Hadzibabic, and W. Ketterle, Phys. Rev. Lett. **83**, 2502 (1999).
[9] C. Ryu, M. F. Andersen, P. Cladé, V. Natarajan, K. Helmerson, and W. D. Phillips, Phys. Rev. Lett. **99**, 260401 (2007).
[10] A. Ramanathan, K. C. Wright, S. R. Muniz, M. Zelan, W. T. Hill, C. J. Lobb, K. Helmerson, W. D. Phillips, and G. K. Campbell, Phys. Rev. Lett. **106**, 130401 (2011).
[11] J. Clark and A. I. Braginski, *The SQUID Handbook* (Wiley-VCH, Weinheim, 2004).
[12] C. Ryu, P. W. Blackburn, A. A. Blinova, and M. G. Boshier, Phys. Rev. Lett. **111**, 205301 (2013).
[13] M. Albiez, R. Gati, J. Fölling, S. Hunsmann, M. Cristiani, and M. K. Oberthaler, Phys. Rev. Lett. **95**, 010402 (2005).
[14] L. Amico, A. Osterloh, and F. Cataliotti, Phys. Rev. Lett. **95**, 063201 (2005).
[15] L. Amico, G. Birkl, M. Boshier, and L.-C. Kwek, New J. Phys. **19**, 063201 (2017).

[16] E. J. Mueller, Phys. Rev. A **66**, 063603 (2002).
[17] S. Eckel, J. G. Lee, F. Jendrzejewski, N. Murray, C. W. Clark, C. J. Lobb, W. D. Phillips, M. Edwards, and G. K. Campbell, Nature (London) **506**, 200 (2014).
[18] S. Baharian and G. Baym, Phys. Rev. A **87**, 013619 (2013).
[19] M. Syafwan, P. Kevrekidis, A. Paris-Mandoki, I. Lesanovsky, P. Krüger, L. Hackermüller, and H. Susanto, J. Phys. B: At. Mol. Opt. Phys. **49**, 235301 (2016).
[20] K. C. Wright, R. B. Blakestad, C. J. Lobb, W. D. Phillips, and G. K. Campbell, Phys. Rev. A **88**, 063633 (2013).
[21] M. Kunimi and I. Danshita, Phys. Rev. A **99**, 043613 (2019).
[22] A. Kumar, S. Eckel, F. Jendrzejewski, and G. K. Campbell, Phys. Rev. A **95**, 021602(R) (2017).
[23] J. H. Kim, S. W. Seo, and Y. Shin, Phys. Rev. Lett. **119**, 185302 (2017).
[24] S. Beattie, S. Moulder, R. J. Fletcher, and Z. Hadzibabic, Phys. Rev. Lett. **110**, 025301 (2013).
[25] N. R. Cooper and Z. Hadzibabic, Phys. Rev. Lett. **104**, 030401 (2010).
[26] R. Lopes, C. Eigen, N. Navon, D. Clément, R. P. Smith, and Z. Hadzibabic, Phys. Rev. Lett. **119**, 190404 (2017).
[27] R. Chang, Q. Bouton, H. Cayla, C. Qu, A. Aspect, C. I. Westbrook, and D. Clément, Phys. Rev. Lett. **117**, 235303 (2016).
[28] A. Weiße and H. Fehske, Exact diagonalization techniques, in *Computational Many-Particle Physics*, edited by H. Fehske, R. Schneider, and A. Weiße, Lecture Notes in Physics Vol. 739 (Springer, Berlin Heidelberg, 2008), pp. 529–544.
[29] J.-W. Lee, J. Korean Phys. Soc. **73**, 325 (2018).
[30] A. U. J. Lode, K. Sakmann, O. E. Alon, L. S. Cederbaum, and A. I. Streltsov, Phys. Rev. A **86**, 063606 (2012).
[31] O. E. Alon, A. I. Streltsov, and L. S. Cederbaum, Phys. Rev. A **77**, 033613 (2008).
[32] L. Pollet, Rep. Prog. Phys. **75**, 094501 (2012).
[33] N. Navon, A. L. Gaunt, R. P. Smith, and Z. Hadzibabic, Science **347**, 167 (2015).
[34] M. Naraschewski and R. J. Glauber, Phys. Rev. A **59**, 4595 (1999).
[35] R. G. Dall, A. G. Manning, S. S. Hodgman, W. RuGway, K. V. Kheruntsyan, and A. G. Truscott, Nat. Phys. **9**, 341 (2013).
[36] S. S. Hodgman, R. I. Khakimov, R. J. Lewis-Swan, A. G. Truscott, and K. V. Kheruntsyan, Phys. Rev. Lett. **118**, 240402 (2017).
[37] R. Roy, A. Gammal, M. C. Tsatsos, B. Chatterjee, B. Chakrabarti, and A. U. J. Lode, Phys. Rev. A **97**, 043625 (2018).
[38] S. I. Mistakidis, L. Cao, and P. Schmelcher, J. Phys. B **47**, 225303 (2014).
[39] A. U. J. Lode, B. Chakrabarti, and V. K. B. Kota, Phys. Rev. A **92**, 033622 (2015).
[40] S. I. Mistakidis, L. Cao, and P. Schmelcher, Phys. Rev. A **91**, 033611 (2015).
[41] S. I. Mistakidis and P. Schmelcher, Phys. Rev. A **95**, 013625 (2017).
[42] J. Neuhaus-Steinmetz, S. I. Mistakidis, and P. Schmelcher, Phys. Rev. A **95**, 053610 (2017).
[43] G. M. Koutentakis, S. I. Mistakidis, and P. Schmelcher, Phys. Rev. A **95**, 013617 (2017).
[44] S. Mistakidis, G. Koutentakis, and P. Schmelcher, Chem. Phys. **509**, 106 (2018).
[45] T. Plaßmann, S. I. Mistakidis, and P. Schmelcher, J. Phys. B **51**, 225001 (2018).
[46] J. H. V. Nguyen, M. C. Tsatsos, D. Luo, A. U. J. Lode, G. D. Telles, V. S. Bagnato, and R. G. Hulet, Phys. Rev. X **9**, 011052 (2019).
[47] S. Klaiman and L. S. Cederbaum, Phys. Rev. A **94**, 063648 (2016).
[48] A. U. J. Lode, Phys. Rev. A **93**, 063601 (2016).
[49] E. Fasshauer and A. U. J. Lode, Phys. Rev. A **93**, 033635 (2016).
[50] J. Erdmann, S. I. Mistakidis, and P. Schmelcher, Phys. Rev. A **98**, 053614 (2018).
[51] L. Cao, S. I. Mistakidis, X. Deng, and P. Schmelcher, Chem. Phys. **482**, 303 (2017).
[52] G. M. Koutentakis, S. I. Mistakidis, and P. Schmelcher, New J. Phys. **21**, 053005 (2019).
[53] S. I. Mistakidis, G. C. Katsimiga, G. M. Koutentakis, and P. Schmelcher, New J. Phys. **21**, 043032 (2019).
[54] M. Cominotti, D. Rossini, M. Rizzi, F. Hekking, and A. Minguzzi, Phys. Rev. Lett. **113**, 025301 (2014).
[55] M. Olshanii, Phys. Rev. Lett. **81**, 938 (1998).
[56] H.-D. Meyer, F. Gatti, and G. A. Worth, *Multidimensional Quantum Dynamics—MCTDH Theory and Applications* (Wiley-VCH, Weinheim, 2009).
[57] A. U. J. L. Lode, M. C. T. Tsatsos, E. Fasshauer, L. P. R. Lin, P. Molignini, C. Lévêque, and S. E. Weiner, MCTDH-X: The Time-Dependent Multiconfigurational Hartree for Indistinguishable Particles software, http://ultracold.org, accessed July 17, 2019.
[58] L. D. Carr, C. W. Clark, and W. P. Reinhardt, Phys. Rev. A **62**, 063610 (2000).
[59] J. Sato, R. Kanamoto, E. Kaminishi, and T. Deguchi, New J. Phys. **18**, 075008 (2016).
[60] A. Muñoz Mateo, A. Gallemí, M. Guilleumas, and R. Mayol, Phys. Rev. A **91**, 063625 (2015).
[61] A. J. Leggett, Phys. Rev. Lett. **25**, 1543 (1970).
[62] K. Sakmann, A. I. Streltsov, O. E. Alon, and L. S. Cederbaum, Phys. Rev. A **78**, 023615 (2008).
[63] X. Yin, Y. Hao, S. Chen, and Y. Zhang, Phys. Rev. A **78**, 013604 (2008).